Epitaxial Core/Shell Nanocrystals of (Europium-Doped) zirconia and hafnia

Carlotta Seno[§], Nico Reichholf[§], Francesco Salutari[†], Maria Chiara Spadaro[†,≠], Yurii P. Ivanov[¶], Giorgio Divitini[¶], Alexander Gogos[¤,#], Inge Herrmann[¤,#], Jordi Arbiol[†,ǂ], Philippe F. Smet[‡] and Jonathan De Roo[§]*

§ Department of Chemistry, University of Basel, Mattenstrasse 24a, 4058 Basel, Switzerland

† Catalan Institute of Nanoscience and Nanotechnology (ICN2), Barcelona 08193 Catalonia, Spain

≠ Department of Physics and Astronomy 'Ettore Majorana', University of Catania, Via S. Sofia 64, 95123 Catania, Italy

¶ Electron Spectroscopy and Nanoscopy, Istituto Italiano di Tecnologia, Via Morego 30, 16163 Genova, Italy

ǂ ICREA, Barcelona 08010 Catalonia, Spain

¤ Laboratory for Particles-Biology Interactions, Department of Materials Meet Life, Swiss Federal Laboratories for Materials Science and Technology (Empa), Lerchenfeldstrasse 5, 9014 St. Gallen, Switzerland

Nanoparticle Systems Engineering Laboratory, Institute of Process Engineering, Department of Mechanical and Process Engineering, ETH Zurich, Sonneggstrasse 3, 8092 Zurich, Switzerland

‡ LumiLab, Department of Solid State Sciences, Ghent University, Krijgslaan 281-S1, Ghent, 9000, Belgium

A careful design of nanocrystal architecture can strongly enhance the nanocrystal function. So far, this strategy faced a synthetic bottleneck in the case of refractory oxides. Here, we demonstrate the epitaxial growth of hafnia shells onto zirconia cores, and pure zirconia shells onto europium doped zirconia cores. The core/shell structures are fully crystalline. Upon shelling, the optical properties of the europium dopant are dramatically improved (featuring a more uniform coordination and a longer photoluminescence lifetime), indicating the suppression of non-radiative pathways. These results launch the stable zirconium and hafnium oxide hosts as alternatives for the established $NaYF_4$ systems.

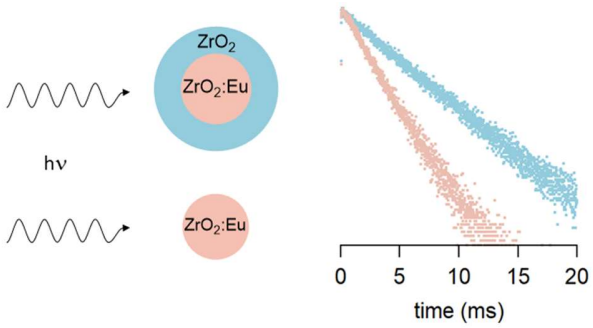

Zirconium and hafnium oxide nanocrystals (NCs) are appealing (host) materials due to their high thermal and chemical stability, and large band gap.[1] Colloidal ZrO_2 NCs are components for (in)organic composites[2-4] while HfO_2 NCs find applications in memory devices.[5, 6] Due to the high atomic number of hafnium and the high density of hafnia, HfO_2 NCs are developed as CT contrast agents,[7-9] scintillators,[10] and as radiation therapy enhancers.[11-13]

Both ZrO_2 and HfO_2 NCs serve as hosts for optically active lanthanide ions, e.g, europium.[1, 14-17] Fluorides (e.g., $NaYF_4$ or $NaGdF_4$) are another class of nanocrystals that are widely used as host for lanthanides with application in both upconversion and downconversion.[18-22] In the fluoride system, the syntheses are well developed, allowing the precise positioning of dopants inside the nanocrystal and the growth of undoped shells on the doped core. This procedure protects the lanthanides from surface effects and thus increases the quantum efficiency of both up- and downconversion processes.[23] Additionally, layered structures offer controlled energy cascades.[24] Higher quantum efficiencies coupled with long lifetimes enabled their use in, e.g., time-gated fluorescence imaging.[15, 25] The oxide hosts have found less widespread use, due to the synthetic challenge of producing colloidally stable oxide nanocrystals with a complex (e.g., core/shell) architecture.[26] However, the oxide hosts are more chemically stable while the fluorides dissolve in highly dilute aqueous media.[27]

Surfactant-assisted, nonaqueous syntheses have allowed to synthesize ZrO_2 and HfO_2 NCs and gain control over their size.[1, 28-34] Even more, solid solutions of various compositions ($Zr_xHf_{1-x}O_2$) were obtained as colloidal nanocrystals.[31, 35, 36] $Hf_{0.5}Zr_{0.5}O_2$ is an interesting ferroelectric material, making it promising for non-volatile memory devices.[37, 38]

Here, we leverage the control of nonaqueous synthesis and report metal oxide core/shell nanocrystals. We epitaxially grow HfO_2 onto ZrO_2, and ZrO_2 onto ZrO_2:Eu^{3+}. The beneficial effect of the shell on the optical properties of the europium dopant is established. Having access to these novel heterostructures (unavailable in bulk) opens up possibilities for

their application in different areas, from microelectronics to scintillators.

Zr and Hf are chemically very similar and both oxide nanocrystals can be synthesized at 340 °C from the metal choride and isopropoxide in tri-*n*-octylphosphine oxide (TOPO).[1] Under these conditions, HfO_2 forms nanorods with the monoclinic crystal structure, while ZrO_2 forms spheres with the tetragonal crystal structure. We first focus on the ZrO_2/HfO_2 core/shell structure, since one can conveniently distinguish growth of HfO_2 onto the spherical ZrO_2 cores from separately nucleating HfO_2 nanorods. ZrO_2 and HfO_2 form similar crystal structures (monoclinic, tetragonal and cubic) with negligible lattice mismatch, thus allowing for epitaxial growth. We follow a two-step approach towards the core/shell structure. In a first step, we synthesize and isolate ZrO_2 cores from $ZrCl_4(THF)_2$ and $Zr(O^iPr)_4.{}^iPrOH$ in TOPO.[39] The cores are spherical, with an average diameter of 3.8 nm according to bright field transmission electron microscopy (BF TEM, Figure 1B). The cores have the tetragonal ($P4_2/nmc$) crystal structure (Figure S1), and their surface is covered with a mixture of protonated TOPO, dioctylphosphinate and dioctyl pyrophosphonate (Figure 1D).[39] In a second step, the purified cores are added to a new reaction mixture of $HfCl_4(THF)_2$ and $Hf(O^iPr)_4.{}^iPrOH$ in TOPO, see Figure 1A.

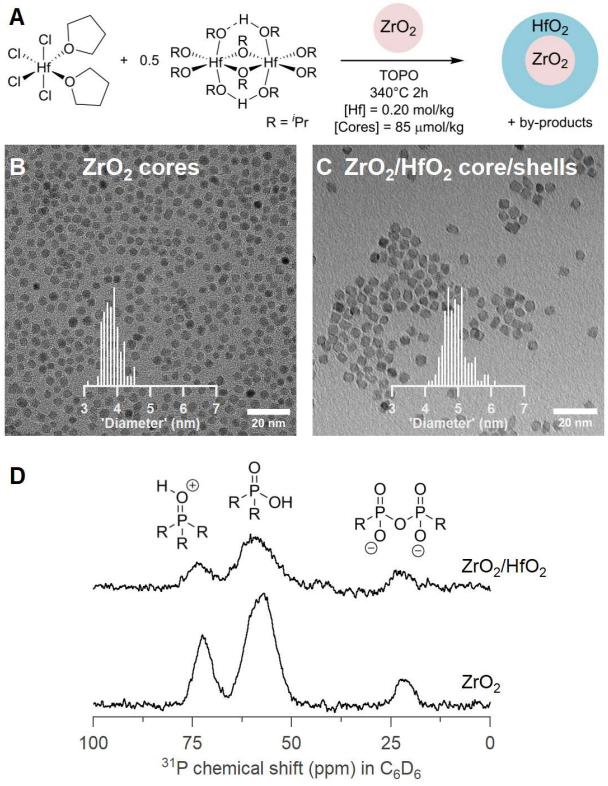

Figure 1. (A) ZrO_2/HfO_2 core/shell synthesis, where $HfCl_4$, THF, propene and isopropanol are obtained as by-products.[28, 29] BF TEM images of (B) ZrO_2 cores and (C) ZrO_2/HfO_2 core/shells. The histograms are based on more than 100 particles. (D) Solution ^{31}P NMR spectra of ZrO_2 and ZrO_2/HfO_2 NCs.

After 2 hours at 340°C, the core/shell structures are isolated and purified. The nanocrystal surface is covered by the same ligands as mentioned before (see Figure 1D for the ^{31}P NMR spectrum). Atomic resolution, high angle annular dark field (HAADF) scanning TEM (STEM) analysis shows that the resulting nanocrystals are no longer spherical, but more clearly faceted, exposing {01-1} and {10-1} surfaces (Figure S2-S3). Nevertheless, to compare to the core diameter, we analyze the BF TEM image (Figure 1C) by measuring the projected area of the faceted nanocrystals and calculate an apparent 'diameter', using the formula of a circle. The core/shell structures have an average 'diameter' of 4.9 nm, clearly indicating that the cores have grown to larger sizes. Crystal growth is further confirmed by the narrower reflections peaks in XRD (Figure S1).

The core/shell interface was further analyzed by atomic resolution HAADF STEM, see Figure 2 (and Figures S2-S3). From the contrast we can recognize the presence of a core/shell structure as the shell appears brighter with respect to the core, due to the higher atomic number of Hf compared to Zr. The power spectrum (FFT) analysis in the reciprocal space, shows that that the ZrO_2 core has the $P4_2/nmc$ tetragonal structure and that the HfO_2 shell has a similar structure. Tetragonal HfO_2 has the following lattice parameters at room temperature: a=b= 3.65 Å, c=5.33 Å, slightly higher than tetragonal ZrO_2 with a=b= 3.59 Å, c=5.18 Å.[40, 41] This is in good agreement with the observed crystal arrangement in our core/shell nanoparticles. The (101) and (10-1) reflections are 'elongated' or doubled, indicating the presence of HfO_2 that grows epitaxially and partially relaxed onto the indicated surfaces of the ZrO_2 core. The frequency filtered map displays clearly the core in green and the shell in red. While pure HfO_2 nanocrystals would crystallize in the monoclinic $P2_1/c$ structure, epitaxial growth thus stabilizes hafnia in its tetragonal structure. Final confirmation of the core/shell structure is provided by energy-dispersive X-ray spectroscopy (EDX) compositional mapping in Figure 2. It shows regions with zirconium in the center and hafnium in the shell.

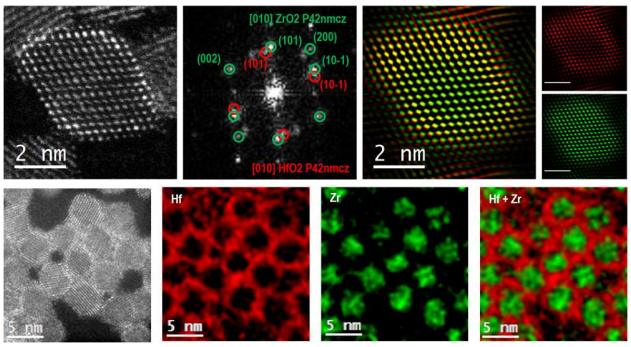

Figure 2. HAADF STEM image of a core/shell ZrO_2/HfO_2 nanocrystal, the corresponding power spectrum (FFT) analysis in the reciprocal space along the [010] zone axis, and the frequency filtered map HAADF STEM image and corresponding EDX compositional maps, featuring hafnium and zirconium.

Second, we turn to the optically active ZrO_2:Eu/ZrO_2 core/shell system. We synthesize europium doped zirconia (10.0% nominal doping) from europium acetate, zirconium propoxide and benzyl alcohol.[15] After synthesis, we functionalize the nanocrystal surface with dodecanoic acid ligands (Figure S4). The ZrO_2:Eu cores have an average diameter of 3.5 nm (Figure 3), possess the tetragonal crystal structure (Figure S1) and have an actual doping concentration of 9.0 % (determined by ICP-OES).

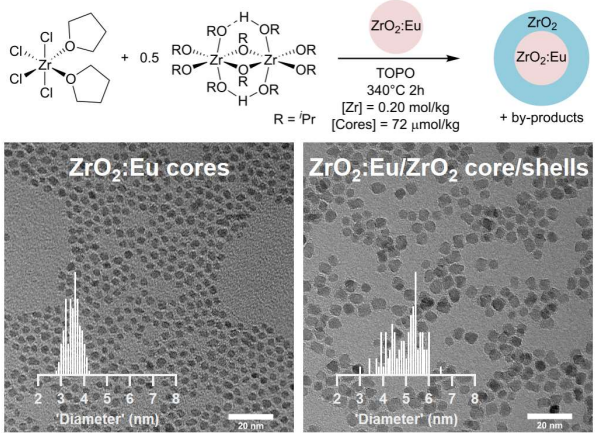

Figure 3: ZrO_2:Eu/ZrO_2 core/shell synthesis, with $ZrCl_4$, THF, propene and isopropanol as by-products.[28, 29] BF TEM images of ZrO_2:Eu cores and ZrO_2:Eu/ZrO_2 core/shells are shown. The histograms are based on more than 100 particles.

The cores were subjected to the shelling procedure using $ZrCl_4(THF)_2$ and $Zr(O^iPr)_4.{}^iPrOH$. After 2 hours at 340°C, colloidally stable nanocrystals were isolated and purified (Figure S5 for ^{31}P NMR and Figure S6 for DLS). BF TEM imaging shows an increase in the average 'diameter' to 5.1 nm (Figure 3) and again sharper reflections are observed in XRD, confirming growth of the tetragonal crystal (Figure S1). HAADF STEM and powder spectrum analysis further confirm that both ZrO_2:Eu cores and ZrO_2:Eu/ZrO_2 core/shells have the tetragonal structure (Figures S7, S8). The europium content decreases in the core/shells to 1.8% metal content. This is close to the expected 2.25% considering the four-fold volume increase of the nanocrystals upon shelling, and also taking into account the limitations in determining the nanocrystal volume given the faceted nature of the core/shell nanocrystals.

The optical properties of the europium dopant change substantially when the cores are shelled, see Figure 4A. The emission spectrum of Eu in the ZrO_2:Eu cores is consistent with previous reports of Eu doped into colloidal ZrO_2 nanocrystals or ZrO_2 powders.[15, 17, 42, 43] Upon shelling, certain transitions disappear and the remaining emission peaks are more narrow. This indicates a change in the coordination around the europium ion. This is further demonstrated by the shape of the $^5D_0$-$^7F_0$ transition around 580 nm, measured at 10K (Figure S9). This J=0 → J'=0 transition is not split by the crystal field, and thus spectrally different contributions for this transition can be assigned to different coordinating environments. For the core/shells, the emission band corresponding to this transition is narrower and more symmetric, indicating a highly uniform environment for europium.

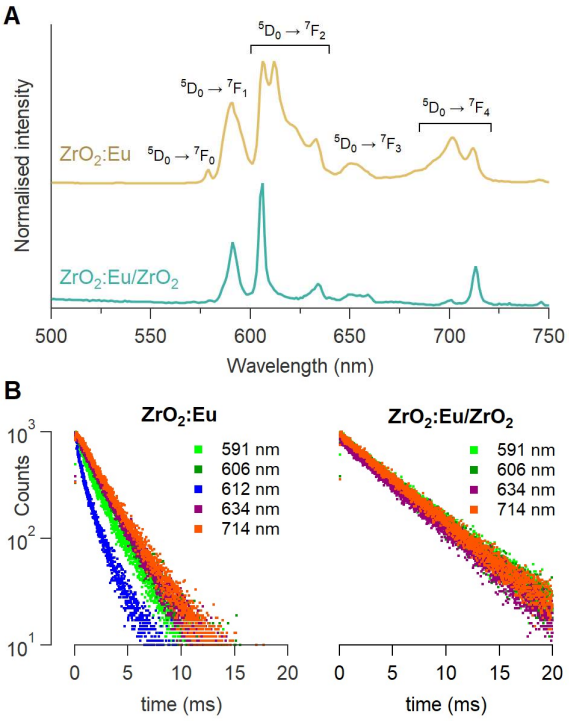

Figure 4: (A) Photoluminescence emission spectra of ZrO_2:Eu cores and ZrO_2:Eu/ZrO_2 core/shells, measured under direct excitation at 394 nm.[44] (B) Lifetime decay at various emission wavelength for both type of particles. Excitation at 238 nm (maximum of charge transfer bands).

The shell has also a big impact on the lifetime of the excited state (Figure 4B). For the ZrO_2:Eu cores, the luminescence decay depends on the monitored wavelength but all feature a biexponential decay. This variation in lifetime points again to different europium coordination environments. We fit the decay using the formula:

$$I(t) = I_0 + a_1 e^{-t/\tau_1} + a_2 e^{-t/\tau_2}$$

At 606 nm, we determine a slow component of 2.7 ± 0.1 ms and a fast component of 1.2 ± 0.1 ms. The slow component contributes 86% to the total emission, calculated via:

$$\phi_1 = \frac{a_1\tau_1}{a_1\tau_1 + a_2\tau_2}$$

For the core/shells, the decay is monoexponential and independent of the monitored wavelength. We determine a lifetime of 5.3 ± 0.1 ms. This is similar to the longest values reported,[45] indicating that the contribution of non-radiative decay, e.g. via interaction with surface or other defects, is limited. In the literature, long lifetimes of 4-5 ms only appear for low doping percentages (1%). Higher doping percentages are typically associated with shorter lifetimes.[45] Here we report a core doped with 9% Eu, which features a lifetime

of 5.3 ms after shelling and thus passivating of the surface defects. Some authors attribute the faster decay to monoclinic crystals phase and the slower decay to the tetragonal phase.[46] Given that we find no evidence for a monoclinic phase, we assign the fast decay for the ZrO_2 cores to Eu ions that are at the nanocrystal surface.

Based on the changes in the emission spectrum and the increase in lifetime, we conclude that the shelling improves the incorporation of the Eu ions in the crystal. Indeed, Eu^{3+} ions act as a probe for their local environment.[44, 47-49]

Finally, we measured the emission spectra of the core/shell particles at low temperatures (Figure S10). When excited at 300 nm, they feature the 4f-4f transitions of Eu^{3+}, and a broadband contribution ranging from 350 nm to 600 nm, related to defect emission in ZrO_2.[28, 50-52] This indicates that the Eu ions remain located in the core during the shelling, since the presence of Eu ions in the shell would suppress the ZrO_2 defect emission (either by preventing the defect to form or by energy transfer to Eu).[53-55] Therefore, the overall emission spectrum of the core/shells contains emission from Eu^{3+} in the core and defect emission from the shells. This also explains the drastic increase in the lifetime of the core/shell particles, since the Eu^{3+} ions are now in a perfect environment far from the outside.

In summary, we reported the use of crystalline zirconium or hafnium oxide to shell nanocrystals. This method was applied to improve the local environment of europium dopants in zirconia nanocrystals and to suppress non-radiative de-excitation pathways. Our results are an invitation to explore intricate nanocrystal architectures with oxide hosts materials.

ASSOCIATED CONTENT

Supporting Information

Description of the synthetic procedures and details of general instrumentation. Characterization of core and core/shell nanoparticles with HAADF STEM, ^{1}H NMR, ^{31}P NMR, DLS and powder XRD.

AUTHOR INFORMATION

Corresponding Author

Jonathan De Roo - Department of Chemistry, University of Basel, Mattenstrasse 24a, 4058 Basel, Switzerland.
Email: jonathan.deroo@unibas.ch

Authors

Carlotta Seno - Department of Chemistry, University of Basel, Mattenstrasse 24a, 4058 Basel, Switzerland.

Nico Reichholf - Department of Chemistry, University of Basel, Mattenstrasse 24a, 4058 Basel, Switzerland.

Francesco Salutari - Catalan Institute of Nanoscience and Nanotechnology (ICN2), Barcelona 08193 Catalonia, Spain.

Maria Chiara Spadaro - Catalan Institute of Nanoscience and Nanotechnology (ICN2), Barcelona 08193 Catalonia, Spain. Department of Physics and Astronomy 'Ettore Majorana', University of Catania, Via S. Sofia 64, 95123 Catania, Italy.

Yurii P. Ivanov - Electron Spectroscopy and Nanoscopy, Istituto Italiano di Tecnologia, Via Morego 30, 16163 Genova, Italy.

Giorgio Divitini - Electron Spectroscopy and Nanoscopy, Istituto Italiano di Tecnologia, Via Morego 30, 16163 Genova, Italy.

Alexander Gogos - Laboratory for Particles-Biology Interactions, Department of Materials Meet Life, Swiss Federal Laboratories for Materials Science and Technology (Empa), Lerchenfeldstrasse 5, 9014 St. Gallen, Switzerland and Nanoparticle Systems Engineering Laboratory, Institute of Process Engineering, Department of Mechanical and Process Engineering, ETH Zurich, Sonneggstrasse 3, 8092 Zurich, Switzerland.

Inge Herrmann - Laboratory for Particles-Biology Interactions, Department of Materials Meet Life, Swiss Federal Laboratories for Materials Science and Technology (Empa), Lerchenfeldstrasse 5, 9014 St. Gallen, Switzerland and Nanoparticle Systems Engineering Laboratory, Institute of Process Engineering, Department of Mechanical and Process Engineering, ETH Zurich, Sonneggstrasse 3, 8092 Zurich, Switzerland.

Jordi Arbiol - Catalan Institute of Nanoscience and Nanotechnology (ICN2), Barcelona 08193 Catalonia, Spain; ICREA, Barcelona 08010 Catalonia, Spain.

Philippe F. Smet - LumiLab, Department of Solid State Sciences, Ghent University, Krijgslaan 281-S1, Ghent, 9000, Belgium.

Notes

The authors declare no competing financial interests.

ACKNOWLEDGMENT

Carlotta Seno and Nico Reichholf thank the SNSF Eccellenza funding scheme (project number: 194172) for funding. The authors acknowledge Jikson Pulparayil Mathew for helping with TGA measurements. ICN2 acknowledges funding from Generalitat de Catalunya 2021SGR00457. This study is part of the Advanced Materials programme and was supported by MCIN with funding from European Union NextGenerationEU (PRTR-C17.I1) and by Generalitat de Catalunya. ICN2 is supported by the Severo Ochoa program from Spanish MCIN / AEI (Grant No.: CEX2021-001214-S) and is funded by the CERCA Programme / Generalitat de Catalunya. Part of the present work has been performed in the framework of Universitat Autònoma de Barcelona Materials Science PhD program. ICN2 is founding member of e-DREAM.[56] Authors acknowledge the use of instrumentation as well as the technical advice provided by the Joint Electron Microscopy Center at ALBA (JEMCA). ICN2 acknowledges funding from Grant IU16-014206 (METCAM-FIB) funded by the European Union through the European Regional Development Fund (ERDF), with the support of the Ministry of Research and Universities, Generalitat de Catalunya. The authors thank Ralf Kägi and Andreas Voegelin (Eawag, Switzerland) for access to their HF-labs.

References

(1) Van den Eynden, D.; Pokratath, R.; De Roo, J. Nonaqueous Chemistry of Group 4 Oxo Clusters and Colloidal Metal Oxide Nanocrystals. *Chem Rev* **2022**, *122* (11), 10538-10572. DOI: 10.1021/acs.chemrev.1c01008.

(2) Tao, P.; Li, Y.; Siegel, R. W.; Schadler, L. S. Transparent dispensible high-refractive index ZrO_2/epoxy nanocomposites for LED encapsulation. *J. Appl. Polym. Sci.* **2013**, *130* (5), 3785-3793. DOI: 10.1002/app.39652.

(3) Liu, C.; Hajagos, T. J.; Chen, D.; Chen, Y.; Kishpaugh, D.; Pei, Q. Efficient one-pot synthesis of colloidal zirconium oxide nanoparticles for high-refractive-index nanocomposites. *ACS applied materials & interfaces* **2016**, *8* (7), 4795-4802.

(4) De Keukeleere, K.; Cayado, P.; Meledin, A.; Vallès, F.; De Roo, J.; Rijckaert, H.; Pollefeyt, G.; Bruneel, E.; Palau, A.; Coll, M. Superconducting $YBa_2Cu_3O_{7-\delta}$ nanocomposites using preformed ZrO_2 nanocrystals: growth mechanisms and vortex pinning properties. *Advanced Electronic Materials* **2016**, *2* (10), 1600161.

(5) Wang, J.; Choudhary, S.; De Roo, J.; De Keukeleere, K.; Van Driessche, I.; Crosby, A. J.; Nonnenmann, S. S. How ligands affect resistive switching in solution-processed HfO_2 nanoparticle assemblies. *ACS applied materials & interfaces* **2018**, *10* (5), 4824-4830.

(6) Maiti, S.; Ohlerth, T.; Schmidt, N.; Aussen, S.; Waser, R.; Simon, U.; Karthäuser, S. Moisture Effect on the Threshold Switching of TOPO-Stabilized Sub-10 nm HfO_2 Nanocrystals in Nanoscale Devices. *The Journal of Physical Chemistry C* **2022**, *126* (43), 18571-18579. DOI: 10.1021/acs.jpcc.2c06303.

(7) McGinnity, T. L.; Dominguez, O.; Curtis, T. E.; Nallathamby, P. D.; Hoffman, A. J.; Roeder, R. K. Hafnia (HfO_2) nanoparticles as an X-ray contrast agent and mid-infrared biosensor. *Nanoscale* **2016**, *8* (28), 13627-13637. DOI: 10.1039/C6NR03217F.

(8) Deblock, L.; Descamps, B.; Goemaere, I.; Goossens, E.; Vergauwen, G.; Debacker, J.; Tummers, P.; Remaut, K.; Van Driessche, I.; De Buysser, K.; et al. Dual-Modality Hafnium Oxide Nanocrystals for in Vivo Computed Tomography and Fluorescence Imaging of Sentinel Lymph Nodes. *Chem. Mat.* **2023**, *35* (21), 8883-8896. DOI: 10.1021/acs.chemmater.3c01324.

(9) Goossens, E.; Deblock, L.; Caboor, L.; Eynden, D. V. D.; Josipovic, I.; Isaacura, P. R.; Maksimova, E.; Van Impe, M.; Bonnin, A.; Segers, P.; et al. From Corrosion Casting to Virtual Dissection: Contrast-Enhanced Vascular Imaging using Hafnium Oxide Nanocrystals. *Small Methods* **2024**, e2301499. DOI: 10.1002/smtd.202301499.

(10) Liu, C.; Hajagos, T. J.; Kishpaugh, D.; Jin, Y.; Hu, W.; Chen, Q.; Pei, Q. Facile Single-Precursor Synthesis and Surface Modification of Hafnium Oxide Nanoparticles for Nanocomposite γ-Ray Scintillators. *Advanced Functional Materials* **2015**, *25* (29), 4607-4616.

(11) Maggiorella, L.; Barouch, G.; Devaux, C.; Pottier, A.; Deutsch, E.; Bourhis, J.; Borghi, E.; Levy, L. Nanoscale radiotherapy with hafnium oxide nanoparticles. *Future oncology* **2012**, *8* (9), 1167-1181.

(12) Marill, J.; Anesary, N. M.; Zhang, P.; Vivet, S.; Borghi, E.; Levy, L.; Pottier, A. Hafnium oxide nanoparticles: toward an in vitropredictive biological effect? *Radiation Oncology* **2014**, *9* (1), 1-11.

(13) Bonvalot, S.; Le Pechoux, C.; De Baere, T.; Kantor, G.; Buy, X.; Stoeckle, E.; Terrier, P.; Sargos, P.; Coindre, J. M.; Lassau, N. First-in-human study testing a new radioenhancer using nanoparticles (NBTXR3) activated by radiation therapy in patients with locally advanced soft tissue sarcomas. *Clinical Cancer Research* **2017**, *23* (4), 908-917.

(14) Villa, I.; Villa, C.; Monguzzi, A.; Babin, V.; Tervoort, E.; Nikl, M.; Niederberger, M.; Torrente, Y.; Vedda, A.; Lauria, A. Demonstration of cellular imaging by using luminescent and anti-cytotoxic europium-doped hafnia nanocrystals. *Nanoscale* **2018**, *10* (17), 7933-7940.

(15) Liu, Y.; Zhou, S.; Tu, D.; Chen, Z.; Huang, M.; Zhu, H.; Ma, E.; Chen, X. Amine-functionalized lanthanide-doped zirconia nanoparticles: optical spectroscopy, time-resolved fluorescence resonance energy transfer biodetection, and targeted imaging. *Journal of the American Chemical Society* **2012**, *134* (36), 15083-15090.

(16) Lauria, A.; Villa, I.; Fasoli, M.; Niederberger, M.; Vedda, A. Multifunctional role of rare earth doping in optical materials: nonaqueous sol–gel synthesis of stabilized cubic HfO_2 luminescent nanoparticles. *Acs Nano* **2013**, *7* (8), 7041-7052.

(17) Ninjbadgar, T.; Garnweitner, G.; Börger, A.; Goldenberg, L. M.; Sakhno, O. V.; Stumpe, J. Synthesis of Luminescent ZrO_2:Eu^{3+} Nanoparticles and Their Holographic Sub-Micrometer Patterning in Polymer Composites. *Adv. Funct. Mater.* **2009**, *19* (11), 1819-1825. DOI: 10.1002/adfm.200801835.

(18) Banski, M.; Afzaal, M.; Podhorodecki, A.; Misiewicz, J.; Abdelhady, A.; O'Brien, P. Passivation of lanthanide surface sites in sub-10 nm $NaYF_4$: Eu^{3+} nanocrystals. *Journal of Nanoparticle Research* **2012**, *14*, 1-10.

(19) Wang, F.; Liu, X. Upconversion multicolor fine-tuning: visible to near-infrared emission from lanthanide-doped $NaYF_4$ nanoparticles. *Journal of the American Chemical Society* **2008**, *130* (17), 5642-5643.

(20) Mai, H.-X.; Zhang, Y.-W.; Si, R.; Yan, Z.-G.; Sun, L.-d.; You, L.-P.; Yan, C.-H. High-Quality Sodium Rare-Earth Fluoride Nanocrystals: Controlled Synthesis and Optical Properties. *J. Am. Chem. Soc.* **2006**, *128* (19), 6426-6436. DOI: 10.1021/ja060212h.

(21) Zheng, B.; Fan, J.; Chen, B.; Qin, X.; Wang, J.; Wang, F.; Deng, R.; Liu, X. Rare-Earth Doping in Nanostructured Inorganic Materials. *Chem. Rev.* **2022**, *122* (6), 5519-5603. DOI: 10.1021/acs.chemrev.1c00644.

(22) Gai, S.; Li, C.; Yang, P.; Lin, J. Recent Progress in Rare Earth Micro/Nanocrystals: Soft Chemical Synthesis, Luminescent Properties, and Biomedical Applications. *Chem. Rev.* **2014**, *114* (4), 2343-2389. DOI: 10.1021/cr4001594.

(23) Rabouw, F. T.; Prins, P. T.; Villanueva-Delgado, P.; Castelijns, M.; Geitenbeek, R. G.; Meijerink, A. Quenching pathways in $NaYF_4$: Er^{3+}, Yb^{3+} upconversion nanocrystals. *ACS nano* **2018**, *12* (5), 4812-4823.

(24) Peng, D.; Ju, Q.; Chen, X.; Ma, R.; Chen, B.; Bai, G.; Hao, J.; Qiao, X.; Fan, X.; Wang, F. Lanthanide-doped energy cascade nanoparticles: full spectrum emission by single wavelength excitation. *Chemistry of Materials* **2015**, *27* (8), 3115-3120.

(25) Hanaoka, K.; Kikuchi, K.; Kobayashi, S.; Nagano, T. Time-resolved long-lived luminescence imaging method employing luminescent lanthanide probes with a new microscopy system. *Journal of the American Chemical Society* **2007**, *129* (44), 13502-13509.

(26) Ramírez-García, G.; Díaz Cervantes, E.; Mounzer, O.; De la Rosa, E.; López Luke, T.; de la Cruz, F. N. A turn-on luminescence method for phosphate determination based on fast green-functionalized ZrO_2: Yb, Er @ ZrO_2 core @ shell upconversion nanoparticles. *Analytical chemistry* **2019**, *91* (22), 14657-14665.

(27) Zhang, F. *Photon Upconversion Nanomaterials*; Springer, 2015.

(28) Joo, J.; Yu, T.; Kim, Y. W.; Park, H. M.; Wu, F. X.; Zhang, J. Z.; Hyeon, T. Multigrarn scale synthesis and characterization of monodisperse tetragonal zirconia nanocrystals. *Journal of the American Chemical Society* **2003**, *125* (21), 6553-6557, Article. DOI: 10.1021/ja034258b.

(29) Pokratath, R.; Van den Eynden, D.; Cooper, S. R.; Mathiesen, J. K.; Waser, V.; Devereux, M.; Billinge, S. J.; Meuwly, M.; Jensen, K. M.; De Roo, J. Mechanistic Insight into the Precursor Chemistry of ZrO_2 and HfO_2 Nanocrystals; towards Size-Tunable Syntheses. *JACS Au* **2022**, *2* (4), 827-838.

(30) Pokratath, R.; Lermusiaux, L.; Checchia, S.; Mathew, J. P.; Cooper, S. R.; Mathiesen, J. K.; Landaburu, G.; Banerjee, S.; Tao, S.; Reichholf, N.; et al. An Amorphous Phase Precedes Crystallization: Unraveling the Colloidal Synthesis of Zirconium Oxide Nanocrystals. *ACS Nano* **2023**, *17* (9), 8796-8806. DOI: 10.1021/acsnano.3c02149.

(31) Tang, J.; Fabbri, J.; Robinson, R. D.; Zhu, Y. M.; Herman, I. P.; Steigerwald, M. L.; Brus, L. E. Solid-solution nanopartieles: Use of a nonhydrolytic sol-gel synthesis to prepare HfO_2 and $Hf_xZr_{1-x}O_2$ nanocrystals. *Chem. Mat.* **2004**, *16* (7), 1336-1342. DOI: 10.1021/cm049945w.

(32) Waetzig, G. R.; Depner, S. W.; Asayesh-Ardakani, H.; Cultrara, N. D.; Shahbazian-Yassar, R.; Banerjee, S. Stabilizing metastable tetragonal HfO_2 using a non-hydrolytic solution-phase route: ligand exchange as a means of controlling particle size. *Chemical Science* **2016**, *7* (8), 4930-4939. DOI: 10.1039/C6SC01601D.

(33) Depner, S. W.; Cultrara, N. D.; Farley, K. E.; Qin, Y.; Banerjee, S. Ferroelastic Domain Organization and Precursor Control of Size in Solution-Grown Hafnium Dioxide Nanorods. *ACS Nano* **2014**, *8* (5), 4678-4688. DOI: 10.1021/nn501632d.

(34) Ohlerth, T.; Du, H.; Hammoor, T.; Mayer, J.; Simon, U. Tailoring of Colloidal HfO2 Nanocrystals with Unique Morphologies and New Self-Assembly Features. *Small Science,* 2300209. DOI: 10.1002/smsc.202300209.

(35) Depner, S. W.; Kort, K. R.; Banerjee, S. Precursor control of crystal structure and stoichiometry in twin metal oxide nanocrystals. *CrystEngComm* **2009**, *11* (5), 841-846.

(36) Robinson, R. D.; Tang, J.; Steigerwald, M. L.; Brus, L. E.; Herman, I. P. Raman scattering in $Hf_xZr_{1-x}O_2$ nanoparticles. *Physical Review B* **2005**, *71* (11), 115408.

(37) Müller, J.; Böscke, T.; Bräuhaus, D.; Schröder, U.; Böttger, U.; Sundqvist, J.; Kücher, P.; Mikolajick, T.; Frey, L. Ferroelectric $Zr_{0.5}Hf_{0.5}O_2$ thin films for nonvolatile memory applications. *Applied Physics Letters* **2011**, *99* (11).

(38) Hwang, J.; Goh, Y.; Jeon, S. Physics, Structures, and Applications of Fluorite-Structured Ferroelectric Tunnel Junctions. *Small* **2023**, 2305271.

(39) De Keukeleere, K.; Coucke, S.; De Canck, E.; Van Der Voort, P.; Delpech, F.; Coppel, Y.; Hens, Z.; Van Driessche, I.; Owen, J. S.; De Roo, J. Stabilization of Colloidal Ti, Zr, and Hf Oxide Nanocrystals by Protonated Tri-n-octylphosphine Oxide (TOPO) and Its Decomposition Products. *Chem Mater* **2017**, *29* (23), 10233-10242. DOI: 10.1021/acs.chemmater.7b04580.

(40) McCormack, S. J.; Weber, R. J.; Kriven, W. M. In-situ investigation of $Hf_6Ta_2O_{17}$ anisotropic thermal expansion and topotactic, peritectic transformation. *Acta Materialia* **2018**, *161*, 127-137.

(41) Lutterotti, L.; Scardi, P. Simultaneous structure and size-strain refinement by the Rietveld method. *Journal of Applied Crystallography* **1990**, *23* (4), 246-252. DOI: 10.1107/S0021889890002382.

(42) Smits, K.; Grigorjeva, L.; Millers, D.; Sarakovskis, A.; Opalinska, A.; Fidelus, J. D.; Lojkowski, W. Europium doped zirconia luminescence. *Optical Materials* **2010**, *32* (8), 827-831.

(43) Nashivochnikov, A. A.; Kostyukov, A. I.; Zhuzhgov, A. V.; Rakhmanova, M. I.; Cherepanova, S. V.; Snytnikov, V. N. Shaping the photoluminescence spectrum of ZrO_2: Eu^{3+} phosphor in dependence on the Eu concentration. *Optical Materials* **2021**, *121*, 111620.

(44) Binnemans, K. Interpretation of europium (III) spectra. *Coordination Chemistry Reviews* **2015**, *295*, 1-45.

(45) Nashivochnikov, A. A.; Kostyukov, A. I.; Rakhmanova, M. I.; Cherepanova, S. V.; Snytnikov, V. N. Photoluminescence and structure evolution of laser synthesized ZrO_2:Eu^{3+} nanopowders depending on the dopant concentration. *Ceram. Int.* **2023**, *49* (3), 5049-5057. DOI: 10.1016/j.ceramint.2022.10.018.

(46) Freris, I.; Riello, P.; Enrichi, F.; Cristofori, D.; Benedetti, A. Synthesis and optical properties of sub-micron sized rare earth-doped zirconia particles. *Optical materials* **2011**, *33* (11), 1745-1752.

(47) Speghini, A.; Bettinelli, M.; Riello, P.; Bucella, S.; Benedetti, A. Preparation, structural characterization, and luminescence properties of Eu^{3+}-doped nanocrystalline ZrO_2. *Journal of Materials Research* **2005**, *20* (10), 2780-2791.

(48) Opitz, L.; Hübner, R.; Shams Aldin Azzam, S.; Gilson, S. E.; Finkeldei, S. C.; Huittinen, N. Investigations towards incorporation of Eu^{3+} and Cm^{3+} during ZrO_2 crystallization in aqueous solution. *Scientific Reports* **2023**, *13* (1), 12276.

(49) Ghosh, P.; Patra, A. Role of surface coating in ZrO_2/Eu^{3+} nanocrystals. *Langmuir* **2006**, *22* (14), 6321-6327.

(50) Emeline, A.; Kataeva, G. V.; Litke, A. S.; Rudakova, A. V.; Ryabchuk, V. K.; Serpone, N. Spectroscopic and photoluminescence studies of a wide band gap insulating material: powdered and colloidal ZrO_2 sols. *Langmuir* **1998**, *14* (18), 5011-5022.

(51) Carvalho, J. M.; Rodrigues, L. C.; Hölsä, J.; Lastusaari, M.; Nunes, L. A.; Felinto, M. C.; Malta, O. L.; Brito, H. F. Influence of titanium and lutetium on the persistent luminescence of ZrO_2. *Optical Materials Express* **2012**, *2* (3), 331-340.

(52) Prakashbabu, D.; Krishna, R. H.; Nagabhushana, B.; Nagabhushana, H.; Shivakumara, C.; Chakradar, R.; Ramalingam, H.; Sharma, S.; Chandramohan, R. Low temperature synthesis of pure cubic ZrO_2 nanopowder: Structural and luminescence studies. *Spectrochimica Acta Part A: Molecular and Biomolecular Spectroscopy* **2014**, *122*, 216-222.

(53) Ponnilavan, V.; Kannan, S. Structural, optical tuning, and mechanical behavior of zirconia toughened alumina through europium substitutions. *Journal of Biomedical Materials Research Part B: Applied Biomaterials* **2019**, *107* (4), 1170-1179.

(54) Villabona-Leal, E.; Diaz-Torres, L.; Desirena, H.; Rodríguez-López, J.; Pérez, E.; Meza, O. Luminescence and energy transfer properties of Eu^{3+} and Gd^{3+} in ZrO_2. *Journal of Luminescence* **2014**, *146*, 398-403.

(55) King, A.; Singh, R.; Nayak, B. B. Phase and photoluminescence analysis of dual-color emissive Eu^{3+}-doped ZrO_2 nanoparticles for advanced security features in anti-counterfeiting. *Colloids and Surfaces A: Physicochemical and Engineering Aspects* **2021**, *631*, 127715.

(56) Ciancio, R.; Dunin-Borkowski, R. E.; Snoeck, E.; Kociak, M.; Holmestad, R.; Verbeeck, J.; Kirkland, A. I.; Kothleitner, G.; Arbiol, J. e-DREAM: the European Distributed Research Infrastructure for Advanced Electron Microscopy. *Microscopy and Microanalysis* **2022**, *28* (S1), 2900-2902.